Chapter 6
Navigation Using CMOS Polarization Sensor

The navigational strategies of insects using skylight polarization are interesting for applications in autonomous agent navigation because they rely on very little information for navigation. The skylight polarization pattern for navigation varies in a systematic fashion both in plane (*e*-vector) and degree of polarization, depending only on the direction of the observation point relative to the angular position of the sun. This is found to be very efficient and reliable for real time navigation.

In this chapter, a polarization navigation sensor using the Stokes parameters to determine the orientation and position is presented. Section 6.1 discusses the two most common navigation algorithms prevalent in most animals: egocentric and geocentric. The working principle of the implemented algorithm is based on egocentric navigation, predominant in insects. The celestial compass based on skylight polarization is presented in section 6.2. Section 6.3 discusses the navigation compass employed by insects and in section 6.4 some of the implemented models for autonomous agent navigation based on the insect's model are presented. In section 6.5 the proposed polarization based compass is presented. The variation in the degree of polarization with changes in the polarized light can be used as a compass and conversely from the degree of polarization the incoming light ray direction can be determined. The computation of ellipticity and azimuthal angles allows for on-chip position detection based on the angle of the incoming light ray with little complexity. This can further be used as a sun position detector based on the skylight polarization. The ability to compute on-chip or in real-time the positional information would result in highly miniaturized navigational sensors.

6.1 Introduction

There are two types of spatial representation created by navigation. One type is a cognitive map or survey representation of space and the other is a route representation [1], [2]. Cognitive mapping or survey representation of the space defines the Euclidean relations (straight line distance and direction) among relevant landmarks within a coordinate reference system centered on the environment.

M. Sarkar and A. Theuwissen: *A Biologically Inspired CMOS Image Sensor*, SCI 461, pp. 185–214.
DOI: 10.1007/ 978-3-642-34901-0_6

Route representation or spatial representation of navigation relies on learning the points in the route.

The role of vision in navigation and cognitive mapping has been extensively studied [3]. Based on the cognitive mapping, navigation can be broadly classified into geocentric and egocentric [3], [4]. Humans navigate using geocentric form of navigation. In geocentric navigation, one uses its cognitive map and its orientation with respect to geocentric coordinates in order to set a course towards a goal. In this case visual cues such as landmarks become very important to generate the cognitive maps. In the absence of information about the location of nearby objects in the environment, humans have difficulty monitoring their travel trajectories, even for short paths. Egocentric navigation, is known to be used by some insect species such as the desert ant *(Cataglyphis fortis)* which relies on path integration, where the movement cues of the navigator are continuously integrated [4]. Animals using egocentric navigation are able to track distance and direction in order to estimate their position even in the absence of visual landmarks.

The progress in the field of autonomous agent navigation has been slower than expected, especially after the initial excitement and rapid advances in the early days of the research [5]. It is interesting to consider why autonomous navigation is so difficult. A survey into the available algorithms for autonomous agent navigation reveals that most of them are written to make them understandable for the human operator, mostly employing Cartesian coordinates *(x,y,z)* to represent the location of the feature [6]. Current sensors employed for navigation applications, and especially robotic navigations, use a generalized algorithm of capturing two-dimension images using a standard CMOS or CCD camera and then processing those captured image sequences for vector calculations to determine the motion vector and the direction vector with reference to the intimal position. The use of image sequences to determine motion and direction vectors is more related to the geocentric form of navigation, where the emphasis is more on the process of creation of two-dimension or three-dimension maps to guide the autonomous agents. This has the advantage of offering more control over the autonomous agent but demands large computational resources and lacks the robustness required for real-time applications. Thus these methods may not be the best solution for artificial autonomous navigation agents.

Insects, on the other hand are able to solve complex navigation problems in real-time relying on egocentric forms of navigation. Thus egocentric forms of navigation is best suited for autonomous agents than the geocentric form. This ability of insects to navigate effortlessly in complex environments without stressing their nervous system has already been a subject of research in robotics, and the cheap computational strategies that these insects use to navigate have been modeled by various researchers [7], [8], [9].

Path integration is the basis of vector navigation in egocentric forms of navigation [10], and it requires knowledge of the direction of travel and the distance travelled. In this book, the focus is on determining the direction of travel and not on distance measurements. To determine the direction of travel a reference direction is needed. The direction is then always expressed relative to the reference. In conventional autonomous agent navigation algorithms, multiple images captured

by a conventional camera and complex image processing algorithms are used to determine the angle of travel [6], [11]. The implementation of these algorithms needs very complex digital logic, and the image processing requires high power consumption and high bus bandwidth [12]. This limits the design of miniature and low-power vision-based navigation systems.

Insects such as the Saharan desert ant *(Cataglyphis fortis)*, use the position of the sun to determine their direction of travel [13]. Since the movement of the sun is constant and equal to approximately 1° every 4 minutes, it serves as a very good directional reference. To determine the direction of travel, ants use the celestial compass either based on the direct sunlight (sun compass) or on the pattern of the polarized skylight (polarization compass) [14]. Santschi [15] was the first to show that ants can use the sun as a compass cue. Genera of ants like *Messor* and *Monomorium* uses sun compass. In *Cataglyphis fortis* the polarization compass dominates over sun compass [14].

To determine the position of the sun using direct sunlight, conventional analog sun position sensors can be used. These sensors measure the position of the sun by allowing the light from the sun to pass through a pin-hole array and illuminate a certain region of the imaging array [16] as shown in figure 6.1.

The position of the illuminated region is then used to compute the altitude and position of the sun with respect to the sensor. State of the art digital sun sensors such

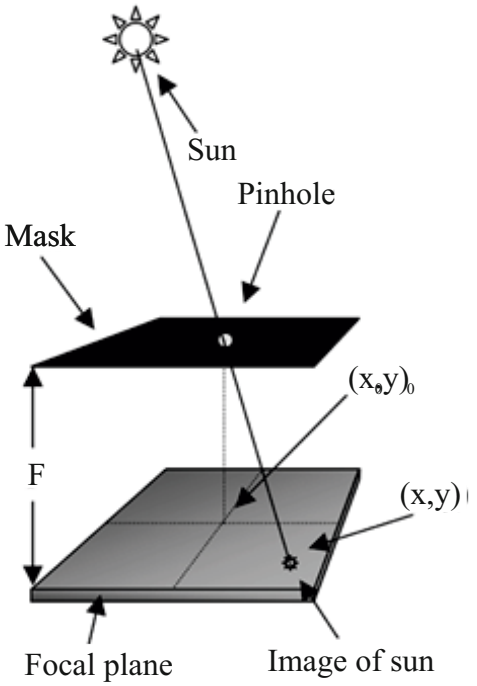

Fig. 6.1 Sun position detection model using image centroid

as [17] use the centroid method to compute the angular position of the sun while row profiling is used in the winner takes all *(WTA)* method proposed by [18]. The prerequisite of these sun sensors is that they need to see the sun, which is not always possible, for example in a cloudy day. Additionally, these sensors need an additional pin-hole array and digital processors to compute the centroid of the obtained image.

The other compass used by insects is the polarization compass. A polarized skylight navigation system uses the extensive pattern of polarized skylight generated by the scattering of the light rays on collision with the air molecules. Each partially polarized skylight ray exhibits a predominant vibration direction (*e*-vector) perpendicular to the plane of the scattering angle. The polarization pattern varies in a systematic fashion both in plane (*e*-vector) and degree of polarization, according to the position of the sun. These polarization patterns in the sky are used by ants as a reference for compass orientation. This makes their navigation pattern completely independent of external visual cues. The celestial compass based on the skylight polarization is described in section 6.2.

6.2 Celestial Compass Based on Skylight Polarization

Direct sunlight is unpolarized. When this unpolarized light enters the earth's atmosphere, it collides with the air molecules or is scattered because of the fluctuations in the air density. The scattering particles, the air molecules, are much smaller than the wavelength of the light striking them, thus the scattered intensity is the same in the forward and the backward directions. This scattering is often explained using the Rayleigh or molecular scattering theory, proposed in 1871 by Lord Rayleigh. The scattering caused by the randomly located air molecules is considered incoherent and thus can be assumed to be coming from only one particle. This scattering is dependent on the wavelength of the incoming light, where intensity of scattering is inversely proportional to the fourth power of the wavelength [19]. Blue light with wavelength at around 425nm scatters 5.5 times more energy than red light of wavelength 650nm. The higher scattering of the blue light explains the blue appearance of the sky.

The scattered light by the air molecules, or skylight, is partially polarized which means it is a composition of both the unpolarized natural light and also a linearly polarized component [20]. Circular and elliptical polarizations, explained in chapter 4, do not usually occur in the sky and thus only the linear polarization component is of interest. The scattered light has an *e*-vector oriented perpendicular to the plane of the scattering, i.e., perpendicular to the great circle passing through the sun and the point observed. Consequently, the *e*-vectors in the sky form concentric circles around the sky. This skylight polarization is mainly dependent on the angle between the viewing direction and the sun and the clearness of the sky in the viewing direction which affects the degree of polarization. There is an indirect relationship between the degree of polarization and the skylight intensity: for sun positions near the zenith, the degree of polarization is quite high while at the horizon the degree of polarization is weaker [21].

The degree of linear polarization is not constant over the entire sky but depends on the solar position of the sun as well as the atmospheric conditions. The strongest linear degree of polarization is observed during the sunrise and sunset at 90° from the sun position. The deeper and clearer the blue of the sky is, the stronger is the degree of polarization. However a total degree of polarization is never observed even when the viewing angle is 90° because secondary scattering and diffuse reflections always reduce the degree of polarization. Clear blue skies are strongly polarized while hazy skies exhibit very little polarization.

In clear sky, the polarization patterns are quite regular and depend very strongly on the position of the sun. The position of the sun in the sky relative to an observer on earth is defined by its solar elevation angle and its solar azimuth angle. The elevation angle is the angle between the line to the center of the sun and the horizontal plane. Horizontal plane is the reference plane for the solar elevation. when the sun is on the horizon, the elevation is 0° while when directly overhead the elevation angle is 90°. The azimuth angle is the angle between true south and the point on the horizon directly below the sun, the reference plane for the solar azimuth is the vertical plane running north-south through the poles. Since the *e*-vector orientation depends only on the plane of the scattering angle, the *e*-vector orientation is nearly independent of the atmospheric disturbance factors. The celestial *e*-vector pattern for two different elevations of the sun is shown in the figure 6.2.

The sun moves along its arc with uniform angular velocity of 15 degrees per hour, while the solar azimuth does not. Its angular velocity depends on the time of day, time of year and geographical latitude. Figure 6.2 shows two distinctive features. First, the gradient of the *e*-vector is related to the position of the sun and second, the pattern of polarization has mirror symmetry with respect to the plane defined by the solar meridian *(SM)* and the anti-solar meridian *(ASM)*. The solar meridian is the line between the sun and the zenith (highest point in the sky). The solar meridian rotates around the zenith as the position of the sun changes. Due to the westward movement of the sun, the *e*-vector pattern rotates around its zenith but retains the two important characteristics over the day, the mirror symmetry and that along the symmetry line the *e*-vectors are always perpendicular to the solar meridian [7].

A model to understand the polarization of the skylight is shown in figure 6.3. The transmission of light from the sun *(S)* to the scatterer *(P)* and the observer *(M)* is shown in the figure. The angle of elevation for the scatterer and the observer are ψ_s and ψ_p respectively.

The parallel and the perpendicular component of the polarized light radiates differently. The perpendicular component radiates omni-directional while the parallel component radiates proportional to $\cos(\psi_p - \psi_s)$ in figure 6.3, the difference of these two components produces the partial polarization of the skylight. The observer views the skylight through the linear polarizer with transmission axis at the angle ζ to the normal of the principal plane (x-axis). As the observer rotates the polarizer, he measures the maximum and minimum in the irradiance. This can be used to compute the degree of polarization [21] as:

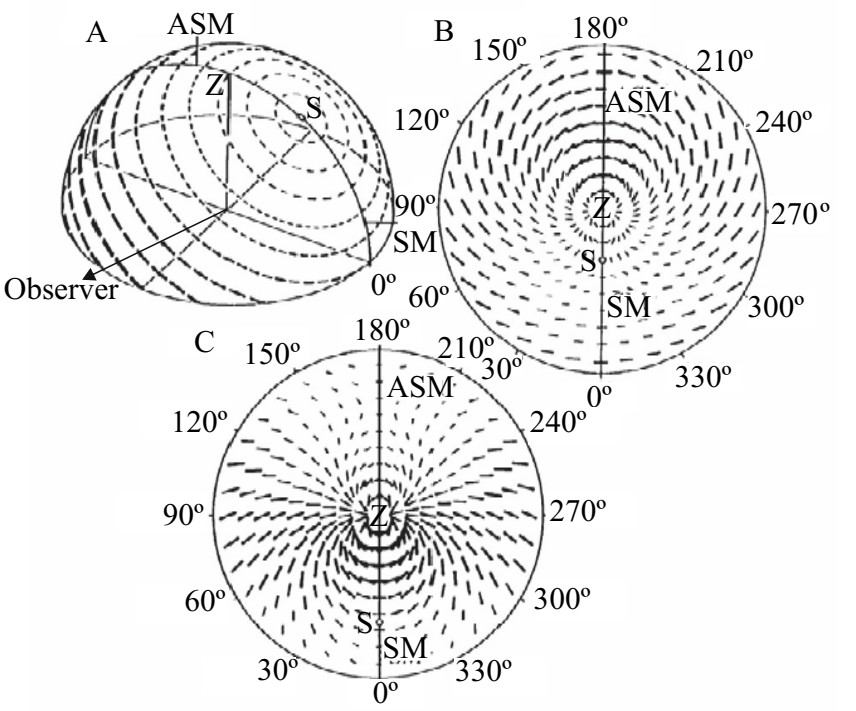

Fig. 6.2 Celestial e-vector pattern (A) Three-dimensional representation of the e-vector pattern, the orientation, length and width of each black bar corresponds to e-vector direction and the degree of polarization respectively. The symmetery line running through sun (S) and zenith (Z), is called "solar meridian" (SM) on the side of the sun and "anti-solar meridian" (ASM) on the opposite side. (B) Two-dimensional for sun elevation at 60° and (C) Two-dimensional for sun elevation at 24°.

$$DOP = \frac{I_{max} - I_{min}}{I_{max} + I_{min}} = \frac{\sin^2(\psi_p - \psi_s)}{1 + \cos^2(\psi_p - \psi_s)} \tag{6.1}$$

where *DOP* is the degree of polarization, I_{max} and I_{min} are the maximum and minimum transmitted intensity, ψ_s and ψ_p are the angle of the sun and the scatterer respectively. This scattered sunlight is partially polarized depending on the scattering angle, the angle between the incoming direct solar light rays and the outgoing skylight rays. The degree of partially linear polarized skylight can be expressed in terms of the scattering angle θ where $\theta = \psi_p - \psi_s$.

The degree of polarization as seen from equation (6.1) only depends on the difference in the angles $\psi_p - \psi_s$. Thus in the direction of the sun, when the scattering angle θ=0° ($\psi_p = \psi_s$), the skylight is completely unpolarized *(DOP=0)*. The maximum degree of polarization *(DOP=1)* would occur for a scattering angle of 90° ($\psi_p = \psi_s + \pi/2$).

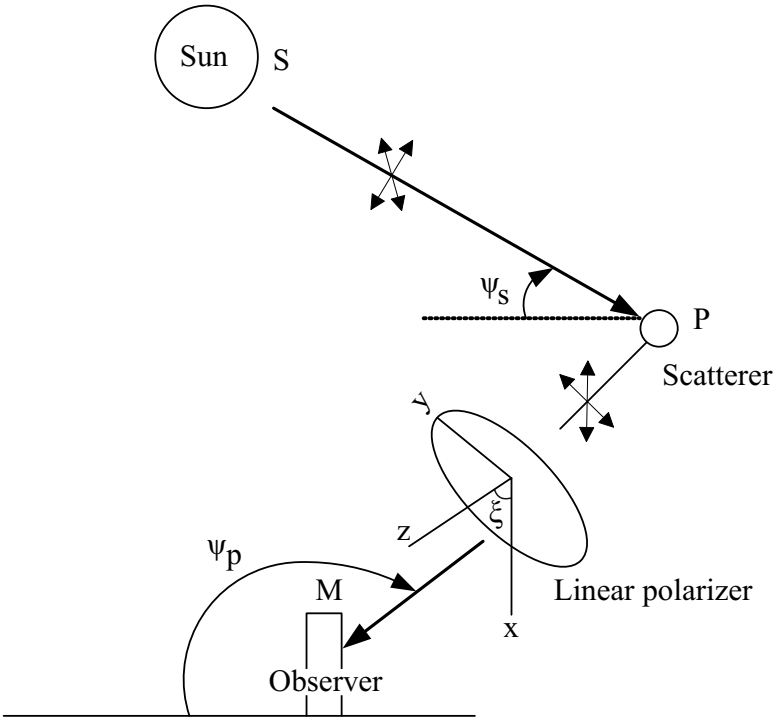

Fig. 6.3 Model to observe the skylight polarization

In figure 6.4, the theoretical degree of linear polarization predicted by equation (6.1) for varying sun elevation angle is plotted along with the measurement results found in literature. For the measurements the observer is viewing the the zenith sky $\psi_p = \pi/2$ as the sun rises (ψ_s increases) in figure 6.3. The two experiments conducted on Mauna Lao in Hawaii [20] and Bocaiuva in Brazil [22] both on high altitudes on a clear day, shows that the measured degree of polarization truly changes with the position of the elevation angle of the sun.

6.3 Navigation Using Polarized Light by Insects

Deserts are barren lands with almost no rain and vegetation. Navigation in such an environment is a challenge due to the absence of any visual landmarks. Humans who rely mostly on geocentric navigation depending on the visual cues and landmarks to form the cognitive map find it difficult to navigate in a desert even with a complex evolved brain. One habitant of such an environment is the Cataglyphis fortis *(Insecta: Hymenoptera: Formincidae)* shown in figure 6.5. For foraging activities such as search of food these ants travel up to twenty thousand times their own body length and go back home in a determined manner straightly without getting lost on the way [23]. This is truly amazing considering the absence of any visual cues or landmarks.

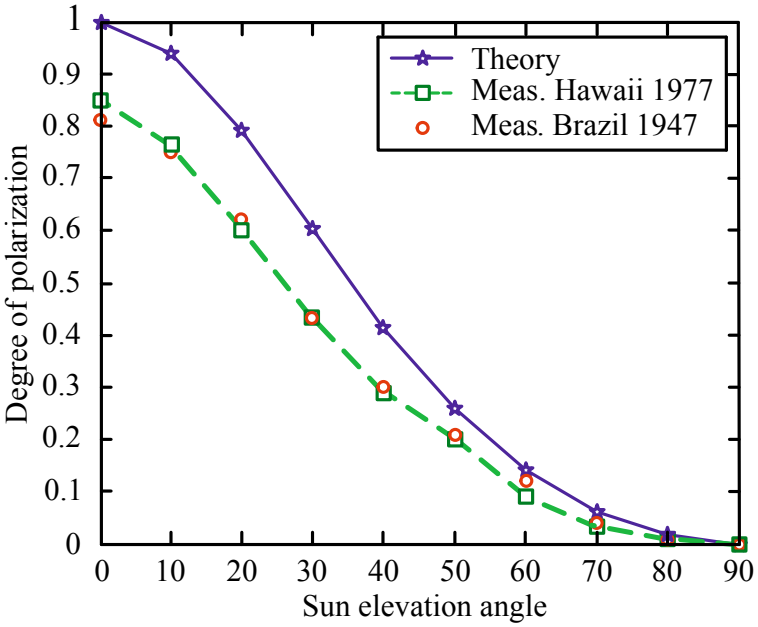

Fig. 6.4 Variation in degree of polarization with changes in the sun elevation angle

Fig. 6.5 Desert ant (Cataglyphis fortis)

Usually when foraging for food ants such as wood ants would mark the route of their travel by placing olfactory marks [24]. This serves two purposes, one to let other ants know the direction towards food and also helps in serving as a return path. This is not possible with Cataglyphis fortis as the sand in the desert is not cohesive

and would be carried away easily by wind. Also the dry environment and the hot surface temperature will evaporate the pheromones too quickly and thus cannot be used for stable marking. The navigation pattern of Cataglyphis fortis has perplexed biologists for a long time and theories about its navigational pattern have been postulated since 1904 when Pieron [25] argued that the ants while homing retrace the steps made during its outward journey by employing certain proprioceptive means. This argument was proven wrong by Cornetz in 1910 [26]. He proposed that the ants integrate their path rather than retrace the steps. This form of navigation is quite similar to that used by sailors at sea before the invention of global positioning system *(GPS)*. This concept of path integration by Cataglyphis fortis is now a widely accepted view [10], [27].

The path integration as the basis of vector navigation requires knowledge of the direction of travel and the distance traveled to compute the home vector. At each stage of foraging the ant continuously updates its home vector which points to the nest of the starting point of the travel. The compound eyes of ants are adapted to detect the polarization prevalent in the skylight [28]. There are three distinct functional regions in the compound eyes of Cataglyphis fortis: the dorsal rim area *(DRA)*, the dorsal area *(DA)* and the ventral area *(VA)* [29]. The microvilli of the *DRA* photoreceptors are aligned in parallel along the entire length of the cell from the distal tip of the rhabdom down to its proximal end and are perpendicular to other microvilli of the other photoreceptor cells [30]. These mutually orthogonal photoreceptors in the microvilli helps to obtain polarization antagonism. The polarization-antagonism has two important effects: it enhances *e*-vector contrast, which allows the neurons to respond to very low degree of polarization and it makes the system insensitive to the variations of absolute light level. That is, the neurons act as differential polarization detectors.

The *e*-vector patterns in the sky are not visible to humans, but ants use these vector directions as a reference for compass orientation. The *e*-vector information collected by the photoreceptors of the *DRA* is processed by polarization sensitive neurons in the optic lobe (*POL* neurons). Although most behavioral studies on the polarization compass are performed in bees and ants, due to the difficulty in recording from ant brains most electrophysiological data are obtained from orthopteran insects like the cricket [31]. The ants' *POL*-neurons exhibit opponency and wide visual fields, like the cricket. The *POL*-neuron of the cricket is shown in the figure 6.6.

The *POL*-neurons receive antagonist inputs from the receptor channels. The response function of the *POL*-neuron is a sinusoidal function of *e*-vector orientation with an excitatory and an inhibitory part and with the maxima and minima separated by 90°. The response function is the difference of the signals from the receptor channels and in principle determines the *e*-vector within the visual field of the neurons.

6.4 Navigation Using Polarized Light for Autonomous Agents

The principle of using polarization antagonism prevalent in the compound eye of insects as a polarization based compass for autonomous agents has been

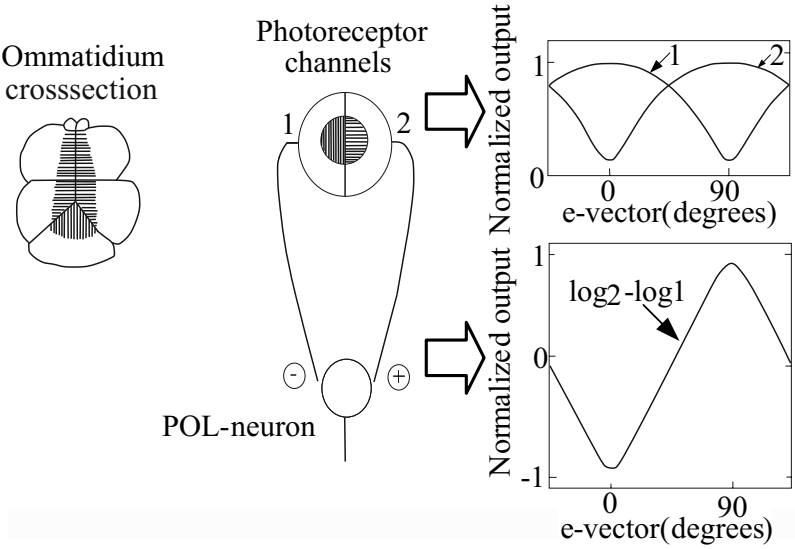

Fig. 6.6 (A) Ommatidum cross section of cricket. (B) Principle of operation of polarization opponent neurons (POL-neurons) [7].

successfully modeled by various researchers. Lambrinos et al. [7], [8] modeled the polarized light sensitive receptors (*POL*-neurons) in the Cataglyphis fortis using a pair of photodiodes with linear polarizers on top and a log ratio amplifier as shown in the figure 6.7. The pair of photodiodes with linear polarizers on top receives mutually orthogonal *e*-vector information, mimicking the receptors in the *DRA* region of the ommatidia of the compound eye of the insects. The response in each of the photodiodes is shifted by 90°. The signal from each diode is then fed to a log amplifier to obtain the logarithmic difference of the intensities received from the two photodiodes, similar in behavior as shown in figure 6.6.

Lambrinos [7] presented an analytical method of determining robot orientation based upon the polarized light neuron receptor geometry of the cricket. The three types of *POL*-neurons in a cricket are tuned to different *e*-vectors oriented approximately 10°, 60° and 130° relative to the length axis of the head. In the model proposed by Lambrinos et al., sensors with maximum sensitivity at the polarizer axis of 0°, 60° and 120° were placed on the robot and analytical expressions for orientation were derived based on models of sensor output. The sensor output was described by the following equation:

$$f(\varphi) = KI[1 + d\cos(2\varphi)] \tag{6.2}$$

where *I* is the total intensity, $I = I_{max} + I_{min}$, I_{max} is the maximum and I_{min} is the minimum intensity obtained from the photodiodes with linear polarizer in crossed-analyzer configuration (the two linear polarizers tuned to orthogonal *e*-vectors),

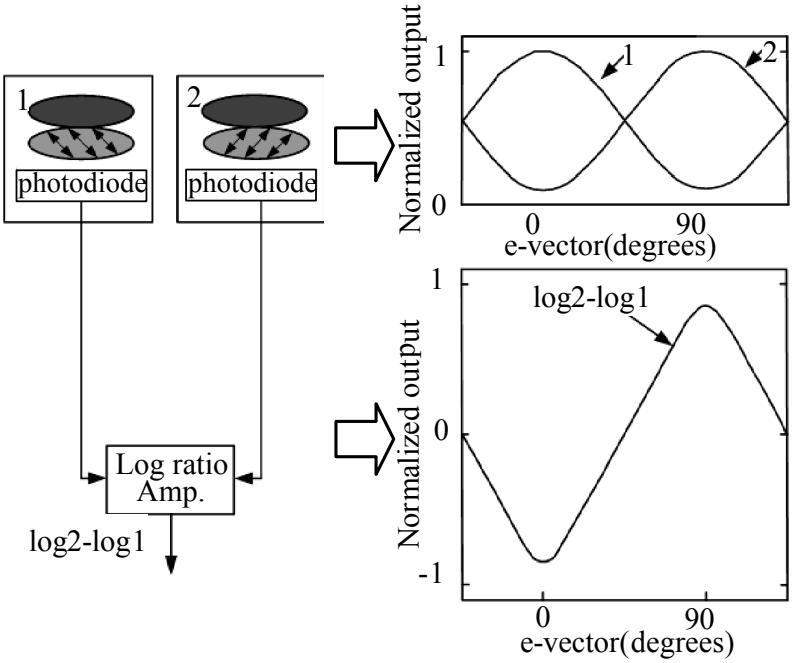

Fig. 6.7 Analog implementation of the POL-neuron [7]

d is the degree of polarization, φ is the orientation with respect to the solar meridian maximizing $f(\varphi)$, and K is a constant [32].

For the three *POL* units oriented at of 0°, 60° and 120° the output of the log amplifier can be expressed as,

$$f_1(\varphi) = \log\left(\frac{1 + d\cos(2\varphi)}{1 - d\cos(2\varphi)}\right) \tag{6.3}$$

$$f_2(\varphi) = \log\left(\frac{1 + d\cos(2\varphi - \frac{2\pi}{3})}{1 - d\cos(2\varphi - \frac{2\pi}{3})}\right) \tag{6.4}$$

$$f_3(\varphi) = \log\left(\frac{1 + d\cos(2\varphi - \frac{4\pi}{3})}{1 - d\cos(2\varphi - \frac{4\pi}{3})}\right) \tag{6.5}$$

where $f_1(\varphi)$, $f_2(\varphi)$ and $f_3(\varphi)$ are the outputs of the *POL* units oriented at 0°, 60°and 120°respectively.

To derive the compass information from equations (6.3), (6.4) and (6.5) either a scanning model or a simultaneous model [7] is used. In the scanning model the first task is to find the solar meridian and use it as a reference direction (0°). The sky is scanned using the system by rotating around its vertical axis to find the maximum.

The maximum value of the output signal is obtained when of the polarization filter is aligned to the solar meridian. After finding the reference direction, the information about the current state of the body can be used to find the direction of motion. In the simultaneous model, a look-up table is used to relate the obtained output values to the orientation and direction of motion instead of scanning the sky for a reference. While scanning the sky the maximum output obtained is used as a reference.

Equation (6.2) is dependent on the degree of polarization. The degree of polarization changes during the day depending on the position of the sun as shown in figure 6.2. In the scanning model of the compass determination, the degree of polarization is naturally eliminated as only the maximum output value is of interest. In the simultaneous model the degree of polarization has to be continuously updated based on the time of day in the look-up table or by normalizing the outputs by first finding the anti-logarithm of the output equations and then applying a sigmoid function. A sigmoid function is a real valued differentiable function whose first derivative is bell shaped and has a single non-negative or non-positive local maximum.

Though Lambrinos et al. in their robots have successfully demonstrated compass detection capability, an important disadvantage of their system is the use of three cameras. Three cameras with 0°, 60° and 120° orientations have to be monitored which is expensive in terms of cost, area, complexity of the algorithm and also the computation power needed to implement the algorithms. Kane et al. [9] proposed a much simpler method where a normal camera with a linear polarization filter is used to take two images, the second image taken with the polarization filter set orthogonal with respect to its position in the first image. From these two images a mean intensity function as a function of polarization angle was derived similar to the form proposed in [7] for the photosensitive diodes.

To solve for the three unknowns in the equation (6.2) Kane et al. use three different images with the polarization transmission axis set to 0°, 45° and 90° respectively. Rearranging equation (6.2) and accounting for images from the different transmission axis, three different image equations can be written.

$$f_1(\varphi) = KI[1 + d\cos(2\varphi)] \tag{6.6}$$

$$f_2(\varphi) = KI[1 + d\cos\left(2\varphi - 2\frac{\pi}{4}\right)] \tag{6.7}$$

$$f_3(\varphi) = KI[1 + d\cos\left(2\varphi - 2\frac{\pi}{2}\right)] \tag{6.8}$$

The set of equations is solved at each pixel of the image to compute the orientation angle φ.

This model also suffers from the disadvantage of using an external linear polarizer which needs to be rotated to have three images with three different transmission axis of the linear polarizer.

Both the models of Lambrinos et al. and Kane et al. are also not very well compensated for the change in the degree of polarization during the day. The models also need an ephemeris compensation algorithm. The ephemeris function is a function that describes the change of the sun's azimuth over time and it depends on the season and the geographical latitude. It is known that the rate of change of the sun's azimuth is not constant: it is faster around noon and slower in the morning. Insects such as bees and ants also suffer from the inherent changes in the ephemeris function but are known to refine their compass detection ability with experience.

6.5 Polarization Based Compass

The models summarized in section 6.4 by Lambrinos et al. and Kane et al. are very similar. The former generates an output image by subtracting the individual image obtained by the two mutually orthogonal photodiodes while the latter generates an output image by adding the two mutually orthogonal images. In the designed image sensor described in this book, these functionalities can be easily incorporated because the individual pixels are polarization sensitive as shown in chapter 4.

6.5.1 Measurement Setup

The measurement setup is the same described in chapter 4. The DC light source generates unpolarized light which is polarized by a linear polarizer. The linear polarized light intensity is then sensed by the imager and the analog output of the imager after digitization using an external *ADC* is fed to the PC for processing. The corresponding analog outputs of the pixels sensitive to 0°, 45° and 90° in the polarization sense regions are used to compute the Stokes parameters.

For the first version of the sensor the Stokes parameters were computed off-chip to have a proof of concept. The circuits required for the computation of Stokes parameters and other digital processing for the implementation of the algorithm can be integrated on chip.

6.5.2 Measurement Results

To validate the functionality as described in section 6.4, the pixel intensities for the 0° and 90° polarization orientation in the two polarization sense regions are recorded. The normalized pixel intensities for 0° and 90° polarization sensitive pixels in sense regions 1 and 2 are shown in figure 6.8. For both polarization sense regions the 0° linear polarizer pixel has the maximum at 0° and the minimum at 90°. Similarly, for the 90° polarizer pixel the maximum is observed at 90° and the minimum at 0°.

To test the compatibility of the designed model with the model used by [7], the logarithmic difference of the mean intensities of the two linear polarizations was

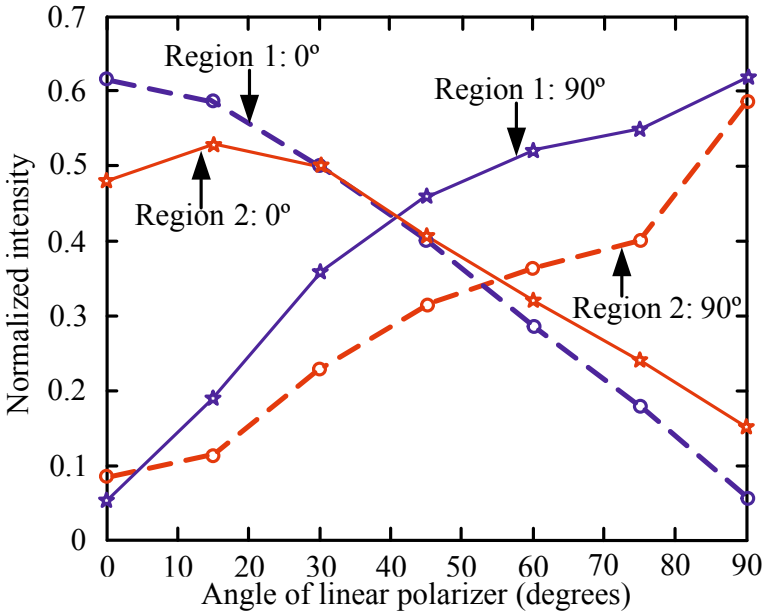

Fig. 6.8 Normalized intensity obtained for 0° and 90° polarization

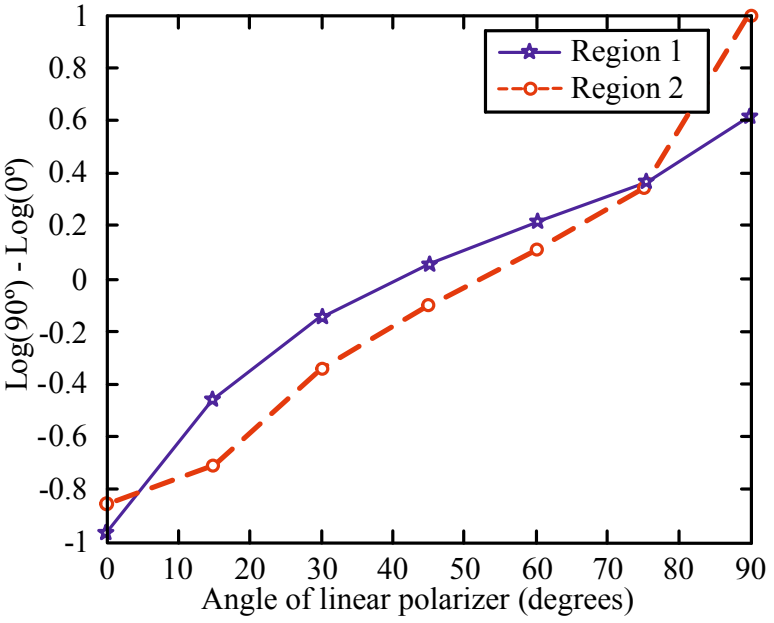

Fig. 6.9 The logarithmic difference of the orthogonal signals in sense region 1 and 2

computed off chip and is plotted in figure 6.9. A very similar characteristic as the one shown by [7] and [8] was achieved for both sense regions.

For both polarization sense regions, the logarithmic difference of the two orthogonal signals was found to have a minimum at 0° linear polarizer angle and a maximum at 90° linear polarizer angle. The logarithmic difference shows an approximately linear increase for increasing linear polarizer angle [33]. This variation in the logarithmic difference can be conceptually used to determine the angle of linear polarization, and based on a reference or look-up table it can be used as a compass.

A different approach is taken here and instead of focusing on polarization differential image or polarization summation image, the variation in the degree of polarization with respect to the orientation of the *e*-vector is studied. The image intensity from the photodiodes in the models described in section 6.4 is a function of the degree of polarization which changes over the course of the day. Lambrinos et al. offsets the effects of the variation in the degree of polarization by normalizing the output and Kane et al. did not compensate for it. The degree of polarization behavior with the orientation angle is evaluated and found that this degree of polarization information can be used to extract the orientation angle and hence can serve as a compass clue.

The variations in the degree of polarization in an image (φ) for changes in the orientation angle φ with respect to the solar meridian is given by equation (6.2). An inverse relationship between the degree of polarization d and the orientation angle φ is obtained.

$$d = \frac{1}{\cos(2\varphi)\left[1 - \frac{f(\varphi)}{KI}\right]} \tag{6.9}$$

Various methods of calculating the degree of polarization from the measured transmitted intensities through the implemented embedded metallic wire grid micro-polarizer have been discussed in chapter 4 and 5. The Stokes degree of linear polarization ((4.22)) is shown in figure 6.10. The degree of polarization calculated using the maximum and minimum transmittance, equation (5.26), is shown in figure 6.11. Both plots show an inverse relationship between *e*-vector orientation angle and the degree of polarization. The Stokes parameters S_1 and S_2 used to calculate the Stokes degree of linear polarization are obtained as:

$$\begin{aligned} S_0 &= {I_{0^\circ}}^2 + {I_{90^\circ}}^2 \\ S_1 &= {I_{0^\circ}}^2 - {I_{90^\circ}}^2 \end{aligned} \tag{6.10}$$

where I_{0° is the intensity of the light after passing through a horizontal linear polarizer, I_{90° is the intensity after a vertical linear polarizer. Figures 6.10 and 6.11 show that both the *DOLP* obtained either by the Stokes parameters or by the *DOP*

obtained from the maximum and minimum transmittance vary between +1 to -1 as the polarizer angle is varied from 0°to 90° [33].

The variations in the degree of linear polarization with respect to the orientation angle can be used as a compass. This approach has the advantage of using fewer computations than the model proposed by Lambrinos et al., where at first the system output was logarithmized and then anti-logarithamized and normalized to remove the dependence on the degree of polarization.

The *DOP* in its simplest form is represented by the Polarization Fresnel Ratio *(PFR)* described in section 5.3.5. The *PFR* is the ratio of the perpendicular Fresnel coefficient to the parallel Fresnel coefficient. The Fresnel coefficients describe the reflection and transmission coefficients of the light wave at an interface. The *PFR* can be roughly estimated as:

$$PFR = \frac{P_{per}}{P_{par}} \tag{6.11}$$

where P_{per} is the power of the perpendicular polarization and P_{par} is the power of the parallel polarization.

The pixel intensities obtained from the pixels covered with wire grid polarizer tilted by 0° and 90° in both sense regions are used to compute the *PFR*. The variation in the *PFR* with varying angle of linear polarizer is shown in figure 6.12.

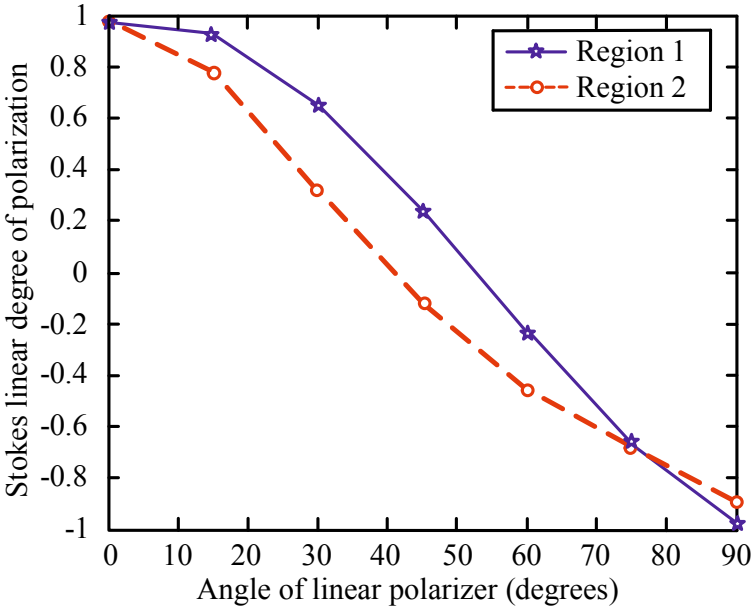

Fig. 6.10 Stokes linear degree of polarization for sense region 1 and 2

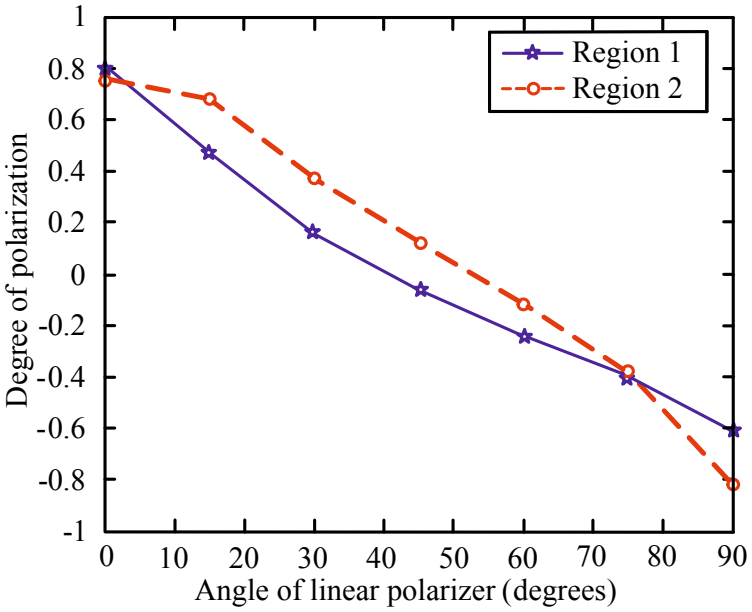

Fig. 6.11 Degree of polarization for sense region 1 and 2

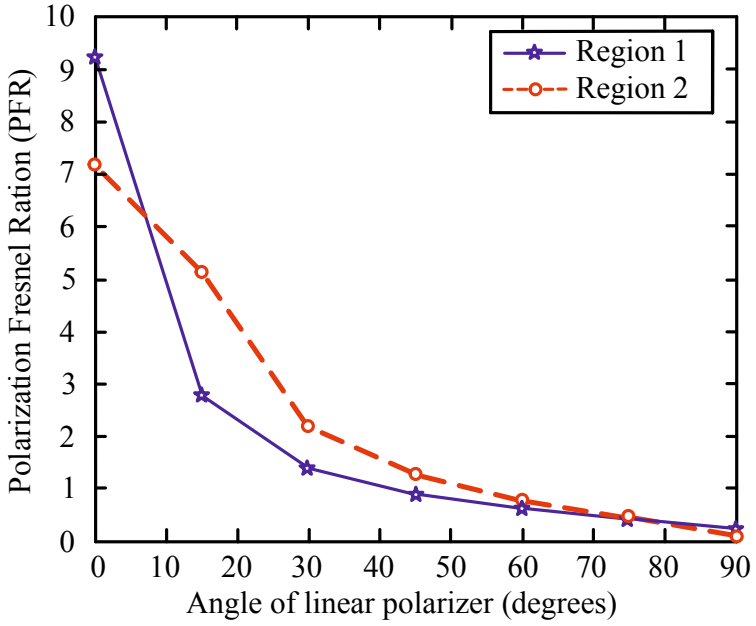

Fig. 6.12 Polarization Fresnel Ratio (PFR) for sense region 1 and 2

From figure 6.12, it is observed that the *PFR* has a maximum value when the polarizer angle is 0° and steadily decreases to a minimum when the polarizer angle is 90° [33]. The decrease is steeper for a lower angle of the linear polarizer than for the higher values. Although the variations in the *PFR* with varying polarizer angle are not linear, the variation for various angles of linear polarizer is still suitable to be used as compass to detect the direction of the incoming polarized light ray.

6.6 Incoming Light Ray Direction Detection and Sun Position Detection

In section 6.5 the variations of the degree of polarization with changes in the orientation angle were observed. In this section it is shown that it is also possible to compute the *e*-vector orientation angle from varying degree of polarization. A polarization navigation sensor principle which uses Stokes parameters to determine the incoming polarized light ray direction is described.

6.6.1 Measurement Setup

The experimental setup shown in figure 6.13 was built for indoor measurements using a DC light source.

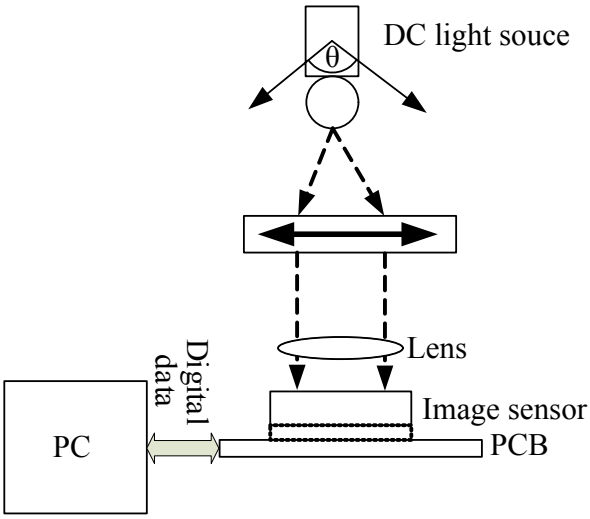

Fig. 6.13 Measurement setup for incoming light ray direction

The measurement setup is very similar to the one described in section 6.5.1, only here the DC light source is not fixed but it can be moved to have an angular direction. The sensor is illuminated with a polarized light obtained by passing the light from

a DC light source through an external linear polarizer. The corresponding analog outputs of the pixels sensitive to 0°, 45° and 90° in the polarization sense regions are recorded. These measurements are then sent to the PC for further processing. For the first version of the sensor the Stokes parameters were computed off-chip to have a proof of concept.

6.6.2 Measurement Results for Incoming Light Ray Directions

The Poincaré sphere described in chapter 4 is used to display the Stokes parameters and is characterized by an ellipticity angle and an azimuthal angle. The ellipticity angle and the azimuthal angle of the Poincar sphere, computed from the Stokes parameters are shown to be correlated with the incoming polarized light ray direction.

6.6.2.1 Incoming Light Ray Direction Detection Using Ellipticity Angle

To measure the ellipticity angle projected by the incoming light ray, the angular position of the DC light source in figure 5.13 was varied to change the incoming light ray direction. Using equations (4.21) and (4.24), the ellipticity angle can be expressed as

$$\chi = \frac{1}{2}\sin^{-1}\left(\frac{S_3}{\delta x S_0}\right) \tag{6.12}$$

where χ is the ellipticity angle, δ is the degree of polarization and S_0 and S_3 are the Stokes parameters. The variation in the measured ellipticity angle with the variation in the angular position of the DC light source is shown in figure 6.14.

The ellipticity angle (χ) as shown in equation (6.12) depends on the degree of polarization. The measured ellipticity angle for 10°, 15° and 30° incidence is shown as "Stokes *DOP*" in figure 6.14, where the degree of polarization is computed using the equation (4.21). The computation of the Stokes degree of polarization from the Stokes parameters needs squaring and square root arithmetic operations. These operations are relatively difficult to implement on-chip.

The calculated ellipticity angle using the partial polarization computed from equation (5.31) is shown as "Partial Polarization" in figure 6.14. This computation is easier to implement on chip as it would only need a differential amplifier to compute the difference and an analog divider. A real time implementation model of an analog divider is discussed in section 6.7. In the skylight polarization only the linear component of the polarization is dominant, and the circular and elliptical polarization components are usually absent. Thus for experiments under open sky, only the linear degree of polarization will be measured. The measurement of the ellipticity angle using the Stokes degree of linear polarization as in equation (4.22) is shown in figure 6.14 as "Linear *DOP*".

The correlation coefficient indicates the strength and direction of a linear relationship between two random variables and can be calculated using equation (6.13)

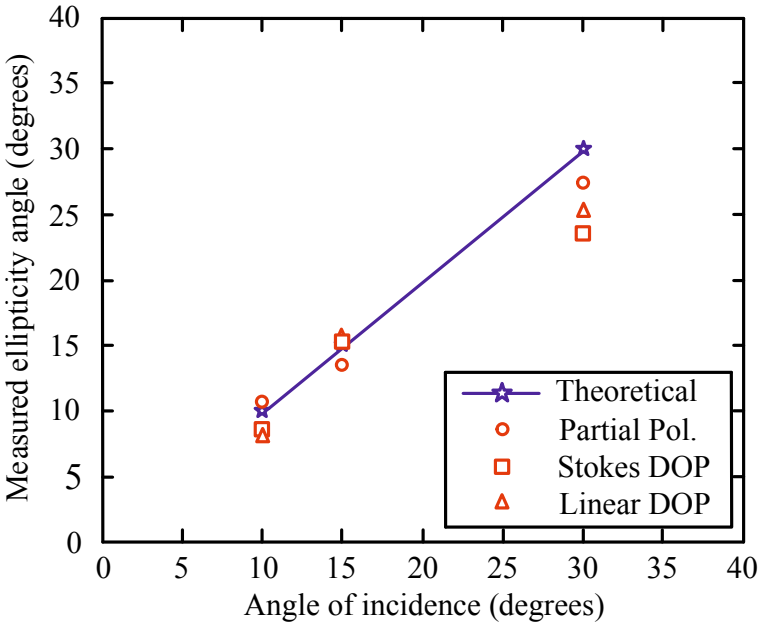

Fig. 6.14 Measurement of incident light ray angle

$$\text{correlation} = \frac{[N\sum xy - \sum x \sum y]}{\sqrt{[N\sum x^2 - (\sum x)^2][N\sum y^2 - (\sum y)^2]}} \tag{6.13}$$

where N is the number of elements and x and y are the two variables.

Correlation coefficients of 0.98, 0.94 and 0.97 are obtained between the theoretical and measured results for Stokes *DOP*, Partial polarization and linear *DOP* respectively [34]. The high values of the correlation coefficients imply a strong correlation between the theoretical and the measured results. Thus the incoming polarized light ray direction can be related to the ellipticity angle of the Poincaré sphere.

6.6.2.2 Incoming Light Ray Direction Detection Using Azimuthal Angle

The azimuthal position (ψ) is computed from the Stokes parameters using equation (4.15) and (4.24). The theoretical and experimentally obtained azimuthal angle in the sense regions 1 and 2, or equivalently, the polarization angle measured while varying the transmission axis of the linear polarizer, is shown in the figure 6.15.

The correlation coefficients of 0.997 and 0.98 in the two regions indicate a strong correlation between the theoretical and the measured results. A linear fit error for the measured angle of linear polarization is computed to be 2.3% and 1.1% in the sense region 1 and 2 respectively [35]. For a similar configuration using an

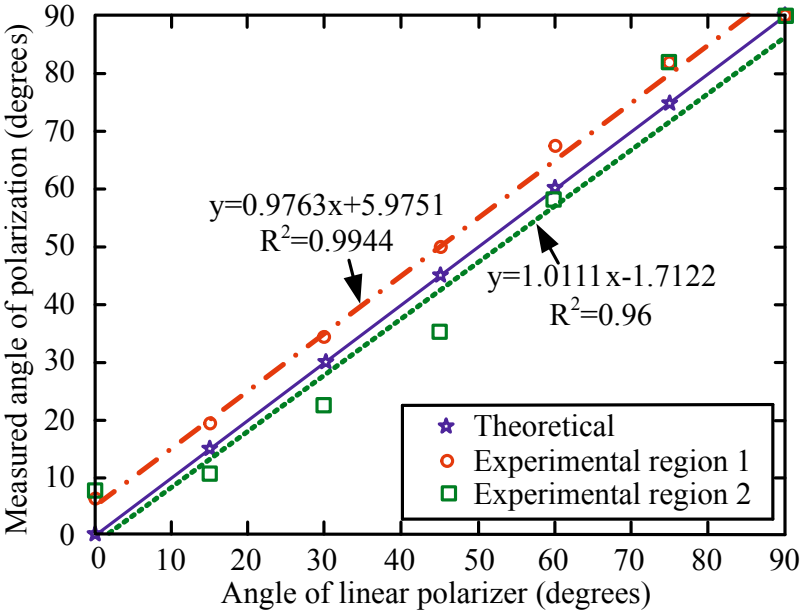

Fig. 6.15 Measured angle of polarization in polarization sense region 1 and 2 using equations (4.15)

organic micro-polarizer, the error is reported to be 2.2% [36] and an error of 1.6% is reported when aluminum nanowires is used with a wire grid pitch of 70nm [37] . The organic micro-polarizer exhibits a very high *ER*, thus the polarization intensity measurements are more accurate. The fabrication of these organic micro-polarizer's require very specialized processes, while the proposed method in this book uses standard CMOS technology processing steps and produces comparable results.

The polarization sense region 2 has an additional 45° linear polarization sensitive pixel (figure 4.32). The Stokes equations are then modified to use the 45° linear polarization information as:

$$\begin{aligned} S_0 &= {I_{0^\circ}}^2 + {I_{90^\circ}}^2 \\ S_1 &= {I_{0^\circ}}^2 - {I_{90^\circ}}^2 \\ S_2 &= {I_{0^\circ}}^2 - {I_{45^\circ}}^2 \end{aligned} \tag{6.14}$$

where I_{0°, I_{90° and I_{45° are the intensity of the light after passing through linear polarizer oriented at 0°, 90°and 45°. The fourth Stokes parameter S_3 is neglected as the light is assumed to be completely linearly polarized. The azimuthal position (ψ) is then computed using equations (4.24) and is shown in figure 6.16.

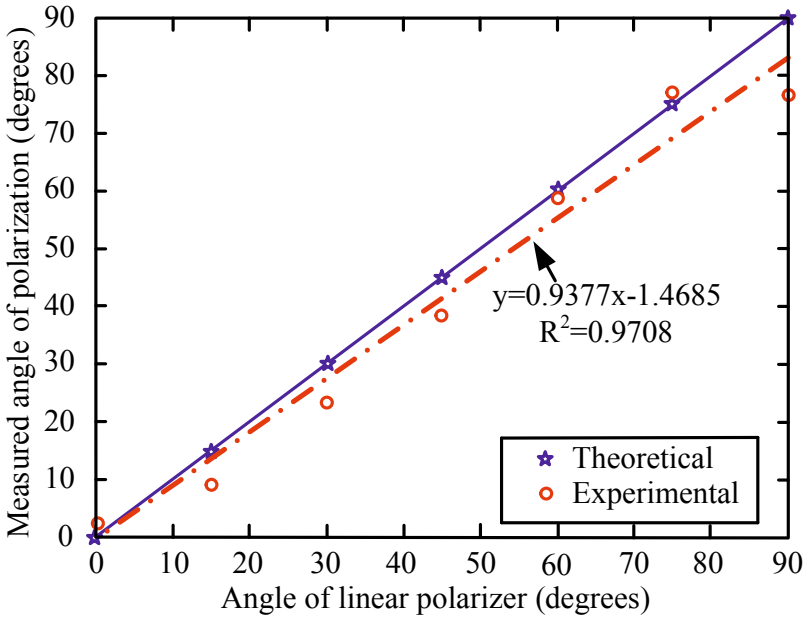

Fig. 6.16 Measured angle of polarization in polarization sense 2 using equations (6.14)

A linear fit error for the angle of linear polarization measurements is computed to be 3.07%. A correlation coefficient of 0.97 is obtained between the theoretical and the experimental values [35].

The Stokes parameters used to obtain the azimuthal position (ψ) in figure 6.15 and figure 6.16 require the computation of the square of the pixel intensities, which is relatively difficult for an on-chip computation. To simplify the computation the Stokes equations can be further simplified as shown in equation (6.15).

$$\begin{aligned} S_{m0} &= I_{0^\circ} + I_{90^\circ} \\ S_{m1} &= I_{0^\circ} - I_{90^\circ} \\ S_{m2} &= I_{0^\circ} - I_{45^\circ} \end{aligned} \tag{6.15}$$

where S_{m0}, S_{m1} and S_{m2} are modified Stokes parameters, computed from the intensities. Equation (4.24) is again used to compute the azimuthal position ψ and is plotted in the figure 6.17.

A linear fit error for the measured angle of linear polarization is computed to be 6%. A correlation coefficient of 0.985 is obtained between the theoretical and the experimental values showing strong correlation [35]. The angular positional information obtained by equations (4.15) and (6.14) is very similar to those obtained by equations (6.15) as shown in the figures 6.16 and 6.17. The equations (6.15) are relatively easy to be implemented on-chip using simple operational amplifiers as

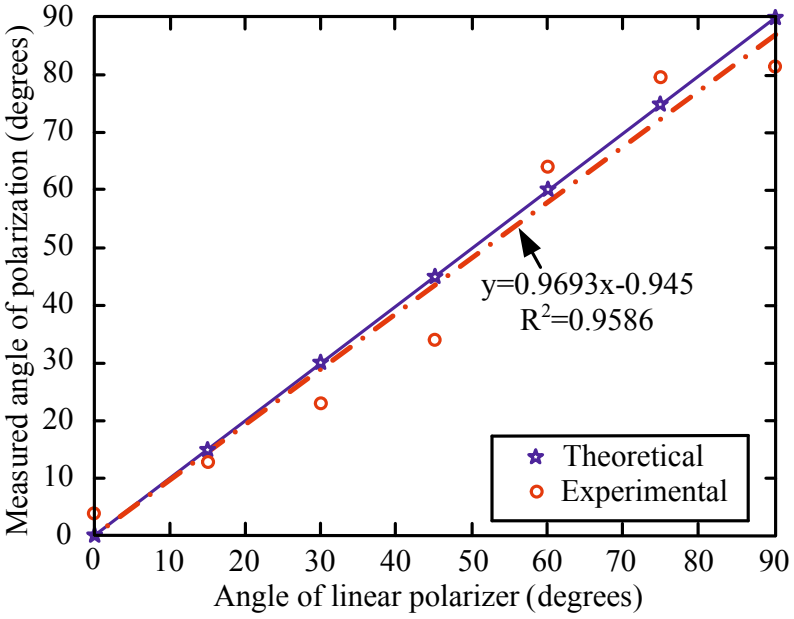

Fig. 6.17 Measured angle of polarization in polarization sense region 2 using equations (6.15)

analog adders or subtractors. The high linearity error is due to the higher metallic wire grid pitch used, limited by the choice of the process technology. With advances in the process technology the pitch can be considerably reduced providing better polarization detection ability and thus a lower linear fit error.

For figures 6.15, 6.16 and 6.17 the transmission axis of the linear polarizer was varied keeping the DC source fixed. The measured azimuthal angles for different angular position of the DC light source in the measurement setup (figure 6.13) for four different measurements are shown in figure 6.18. Similar to the ellipticity angle measurements, the angular position of the light source, and hence the angle of incidence of the light, was varied by 10°, 15° and 30°. A mean correlation coefficient of 0.9904 is obtained between the theoretical and the four measured results [38].

6.7 Real-Time Implementation of Navigation Compass

In section 6.5, it was shown that the polarization Fresnel ratio (PFR) is a good tool to be used as a compass for autonomous agent navigations. To implement the *PFR* calculations in real time using equation (6.11), an analog divider is needed. An analog divider can be implemented either in current mode or in voltage mode using a voltage controlled resistor as shown in figure 6.19 [39]. A current mode analog divider is discussed in this section. To use the current mode analog divider, the voltage at the floating diffusion node of the photodiode needs to be converted to

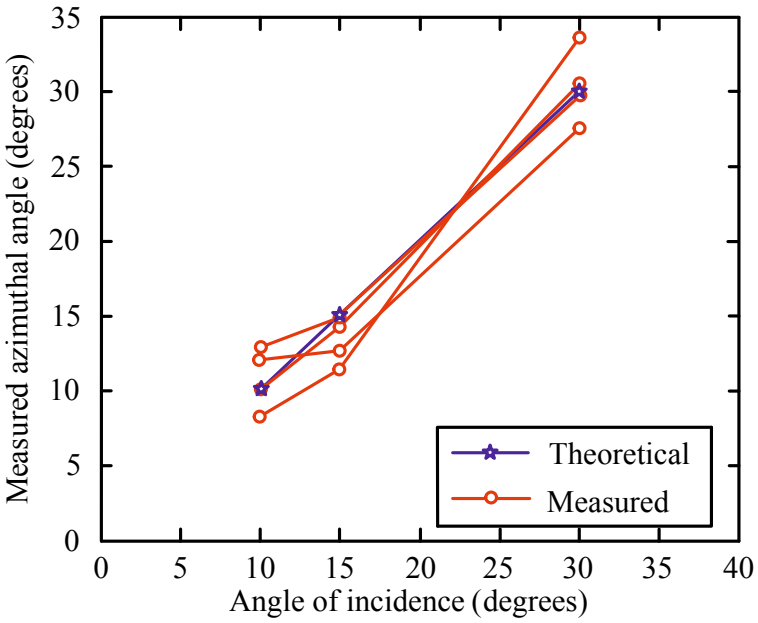

Fig. 6.18 Measurement of incident light ray angle

current. This can be done using a transconductance amplifier or a *V-I* converter. If a conventional *p-n* junction photodiode is used then the photodiode current can directly be copied.

To implement an analog divider, a voltage controlled resistor *(VCR)* is required, an implementation of *VCR* is shown in figure 6.19. If transistors M1 and M2 are biased in triode region then the drain currents I_1 and I_2 are given by:

$$I_1 = I_{in} + I_3 = \frac{K_{n1}}{2}\left(2(V_1 - VTH1)V_{DS1} - V_{DS1}^2\right) \tag{6.16}$$

$$I_2 = \frac{K_{n2}}{2}\left(2(V_2 - VTH2)V_{DS2} - V_{DS2}^2\right) \tag{6.17}$$

where k_{n1} and k_{n2} are the transconductance parameters, V_1, and V_2 are the bias voltages, V_{DS1} and V_{DS2} are the drain to source voltage, V_{TH1} and V_{TH2} are the threshold voltages for the transistors M_1 and M_2 respectively, I_{in} is the additional injected current and I_3 is the drain current of transistor M_3.

The current mirror M_5 and M_6 ensures that I_3 and I_4 have the same value. The current I_4 also passes through the transistor M_2 so that

$$I_3 = I_4 = I_2 \tag{6.18}$$

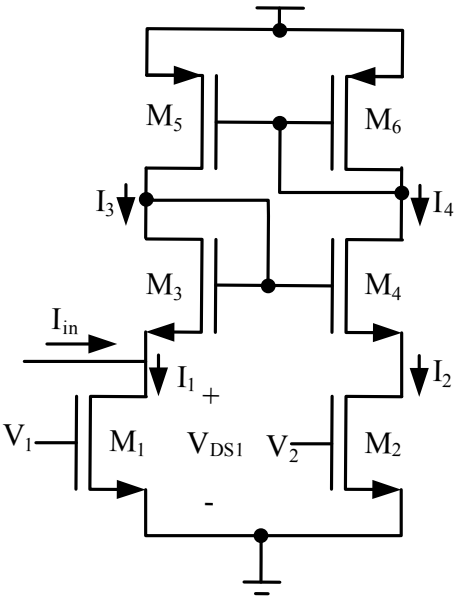

Fig. 6.19 Voltage controlled resistor

Assuming M_3 and M_4 to be perfectly matched and biased in saturation, V_{GS3} is expressed as:

$$V_{GS3} = V_{GS4} = \sqrt{\frac{2I_2}{K_{n4}}} + V_{TH4} \tag{6.19}$$

Also

$$V_{GS4} + V_{DS2} = V_{DS1} + V_{GS3} \tag{6.20}$$

From equations (6.19) and (6.20)

$$V_{DS2} = V_{DS1} \tag{6.21}$$

Substituting equations (6.21), (6.18) and (6.17) in (6.16) and assuming the transistors M_1 and M_2 to be completely matched ($V_{TH1} = V_{TH2} = V_{TH}$ and $K_{n1} = K_{n1} = K_n$), I_{in} can be written as:

$$I_{in} = K_n V_{DS1}(V_1 - V_2) \tag{6.22}$$

From equation (6.22) a voltage controlled resistor between I_{in} and ground can be realized with an equivalent resistance of

$$R_{eq} = \frac{V_{DS1}}{I_{in}} = \frac{1}{K_n(V_1 - V_2)} \tag{6.23}$$

Using the voltage controlled resistor of figure 6.19a current mode divider can be implemented as shown in figure 6.20 [40].

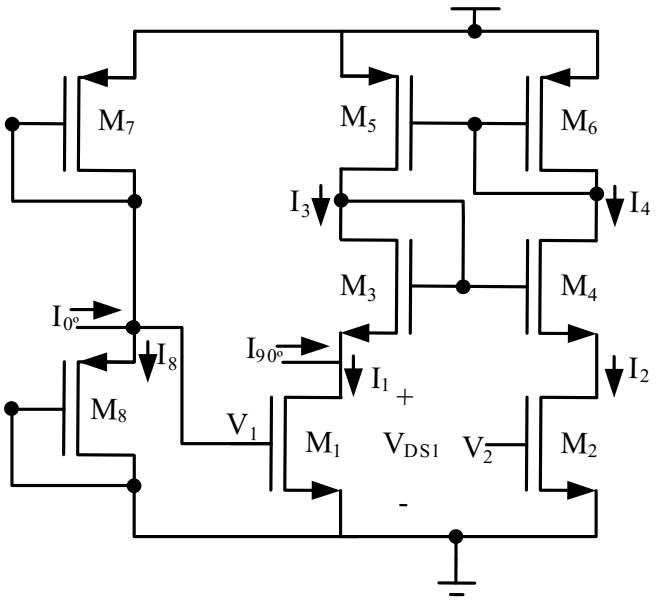

Fig. 6.20 Current mode divider using voltage controlled resistor

Assuming transistors M_7 and M_8 to be perfectly matched ($K_{p7} = K_{p8} = K_p$ and $V_{THP7} = V_{THP8} = V_{THP}$), V_1 can be expressed as:

$$V_1 = \frac{I_{0^\circ}}{2K_p(-V_{THP})} \tag{6.24}$$

Substituting equation (6.23) in (6.21) and grounding V_2

$$V_{DS1} = \frac{2K_p(-V_{THP})}{K_n} \times \frac{I_{90^\circ}}{I_{0^\circ}} \tag{6.25}$$

According to equation (6.25) the output V_{DS1} is proportional to the ratio of the two input currents I_{90° and I_{0° which are the outputs of the two pixels sensitive to 0° and 90° sensitive pixels in the designed image sensor. This allows calculation of the *PFR* in continuous time.

Besides the requirement of an analog divider, the simplified Stokes parameter calculations in equation (6.15) also need a subtraction of the two pixel values which can be easily obtained using the circuit shown in figure 6.21.

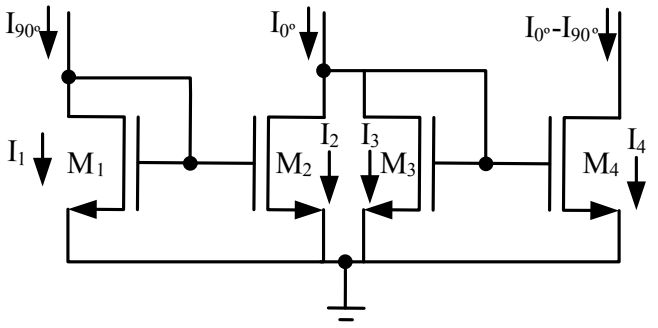

Fig. 6.21 Current mode subtraction circuit

If transistors M_1, M_2, M_3 and M_4 are in saturation, and assuming they are perfectly matched the currents in these two transistors are given by

$$I_1 = I_{90^\circ} = I_2 = \frac{K_n}{2}(V_{GS1} - V_{TH})^2 \tag{6.26}$$

$$I_3 = I_{0^\circ} - I_{90^\circ} \tag{6.27}$$

Since M_3 and M_4 acts as a current mirror the current I_3 is copied by the transistor M_4 and the output current is the difference of the two input currents from the two pixels sensing 0° and 90° polarization.

6.8 Summary

- There are two types of spatial representation created by navigation, one is cognitive map or survey representation and the other is route representation or spatial representation.
- The navigation can be broadly classified as geocentric and egocentric based on the cognitive mapping.
- Human use geocentric navigation wherein the visual clues such as landmarks play an important role. Insects use egocentric navigation, wherein the direction of travel is determined from the position of the sun or from skylight polarization.
- The egocentric navigation is best suited for autonomous agents like robotic navigation as it does not involve large frame to frame image computations to determine the distance and direction of travel.
- Path integration is the basis of vector navigation in egocentric forms of navigation, it requires knowledge of the direction of travel and the distance traveled.

- To determine the direction of travel, a reference direction is needed. Insects use the position of the sun as the reference and compute their travel direction with respect to the position of the sun. The movement of the sun is constant and is approximately 1°every 4 minutes.
- The skylight polarization is also used to determine the reference direction. The skylight polarization is dependent on the position of the sun.
- The skylight polarization pattern varies in a systematic fashion both in plane (*e*-vector) and degree of polarization, according to the position of the sun.
- There exists an indirect relationship between the degree of polarization and the skylight intensity: for sun positions near the zenith, the degree of polarization is quite high while at the horizon the degree of polarization is weaker.
- The principle of using polarization antagonism prevalent in the compound eye of insects as a polarization based compass for autonomous agents has been successfully modeled by various researchers.
- From the micro-polarizer orientations, intensities can be used to calculate the degree of polarization and polarization Fresnel ratio for varying angle of the incoming light which can be used as a compass. The positional information can also be retrieved using Stokes parameters.
- The sun position detection using polarized light would have an advantage over conventional sun position detection sensors as it would work even when the sun is not visible.
- The Stokes parameters are used to compute the ellipticity and azimuthal angles of the perceived light ray, which is correlated to the incoming light ray direction.
- The simplified computational algorithms allow on-chip processing which would result in miniaturized navigational sensors. Such navigational sensor would be independent of the visual cues and use natural light to determine the directional reference.

References

[1] O'keefe, J., Nadel, L.: The Hippocampus as a Cognitive Map. Oxford University Press (1978) ISBN: 0198572069

[2] Thorndyke, P., Hayes-Roth, B.: Differences in spatial knowledge acquired from maps and navigation. Cognitive Psychology 14, 560–589 (1982)

[3] Hafner, V.: Adaptive Navigation Strategies in Biorobotics: Visual Homing and Cognitive Mapping in Animals and Machines. Shaker Verlag (2004) ISBN: 3832228578

[4] Wehner, R., Michel, B., Antonsen, P.: Visual navigation in insects: coupling of egocentric and geocentric information. Journal of Experimental Biology 199, 129–140 (1996)

[5] Moravec, H.: Obstacle avoidance and navigation in the real world by a seeing robot rover. Technical Report CMU-RI-TR-3, Carnegie-Mellon University, Robotic Institute (1980)

[6] DeSouza, G., Kak, A.: Vision for mobile robot navigation: A survey. IEEE Transactions on Pattern and Machine Intelligence 24, 237–267 (2002)

[7] Lambrinos, D., Möller, R., Labhart, T., Pfeifer, R., Wehner, R.: A mobile robot employing insect strategies for navigation. Robotics and Autonomous Systems 30(2), 39–64 (2000)
[8] Lambrinos, D., Maris, M., Kobayashi, H., Labhart, T., Pfeifer, R., Wehner, R.: An autonomous agent navigating with a polarized light compass. Adaptive Behaviour 6(1-2), 131–161 (1997)
[9] Usher, K., Ridley, P., Corke, P.: A camera as a polarized light compass: preliminary experiments. In: Proceedings of Australian Conference on Robotics and Automation, pp. 116–120 (2001)
[10] Müller, M., Wehner, R.: Path integration in desert ants, Cataglyphis Fortis. Proceedings of National Academy of Sciences 85, 5287–5290 (1988)
[11] Chen, Z., Birchfield, S.: Qualitative vision based mobile robot navigation. In: Proceedings of IEEE International Conference on Robotics and Automation, pp. 2686–2692 (2006)
[12] Moini, A.: Vision chips. Kluwer academic publishers, Boston (2002) ISBN: 0792386647
[13] Müller, M., Wehner, R.: The hidden spiral: systematic search and path integration in desert ants, Cataglyphis Fortis. Journal of Comparitive Physiology A-Sensory Neural and Behavioural Physiology 175, 525–530 (1994)
[14] Wehner, R., Müller, M.: The significance of direct sunlight and polarized skylight in the ant's celestial system of navigation. Proceedings of the National Academy of Sciences, USA 103(33), 12575–12579 (2006)
[15] Santschi, F.: Review Suisse Zoology, vol. 19, pp. 303–338 (1911)
[16] Liebe, C.: Solar compass chip. IEEE Sensors Journal 4, 779–786 (2004)
[17] Chang, Y., Kang, S., Lee, B.: High accuracy image centroding algorithm for CMOS based digital sun sensors. In: Proceedings of IEEE Sensors Conference, pp. 329–336 (2007)
[18] Xie, N., Theuwissen, A., Wang, X.: A CMOS image sensor with row and column profiling means. In: Proceedings of IEEE Sensors Conference, pp. 1356–1359 (2008)
[19] Bjorn, L.: Photobiology: the science of life and light, p. 18. Springer publications (2007) ISBN: 9780387726540
[20] Coulson, K.: Polarization and Intensity of Light in the atmosphere, Deepak, Hampton, VA, p. 2 (1988) ISBN: 0937194123
[21] Smith, G.: The polarization of skylight: An example from nature. American Journal of Physics 75(1), 25–35 (2007)
[22] Richardson, R., Hulburt, E.: Sky-brightness measurements near bocaiuva, brazil. Journal of Geophysics Research 54, 215–227 (1949)
[23] Wehner, R.: Desert ant navigation: how miniature brains solve complex task. Journal of Comparitive Physiology A-Sensory Neural and Behavioural Physiology 189, 579–588 (2003)
[24] Seidl, T.: Ant navigation and path finding. In: Proceedings of the 2nd ACT Workshop on Innovative Concepts, vol. 31(4), pp. 102–110 (2008)
[25] Pieron, H.: Du role du sens musculaire dans l'orientation de quelques espéces de fourmis. Bulletin of Institute of General Psychology 4, 168–186 (1904)
[26] Cornetz, V.: Trajets de fourmis et retours au nid. Mémoire De l'Institute Géneral, Psychologie 2, 1–67 (1910)
[27] Mittelstaedt, M.L., Mittelstaedt, H.: Homing by path integration in a mammal. Naturwissenschaften 67, 566–567 (1980)
[28] Wehner, R.: The ant's celestial compass system: spectral and polarization channels. In: Orientation and Communication in Arthropods, pp. 145–185. Birkhäuser Verlag, Basel (1997)

[29] Labhart, T., Meyer, E.: Detectors for polarized skylight in insects: a survey of ommatidial specializations in the dorsal rim area of the compound eye. Microscopy Research and Technique 47, 368–379 (1999)
[30] Herrling, P.: Regional distribution of three ultrastructural retinula types in the retina of cataglyphis bicolor fabr (formicidae, hymenoptera). Cell Tissue Research 69, 247–266 (1976)
[31] Labhart, T.: How polarization-sensitive interneurons of crickets see the polarization pattern of the sky: a field study with an opto-electronic model neuron. Journal of Experimental Biology 202, 757–770 (1999)
[32] Bernard, G., Wehner, R.: Functional similarities between polarization vision and color vision. Vision Research 17, 1019–1028 (1977)
[33] Sarkar, M., Segundo, D.S., van Hoof, C., Theuwissen, A.: Integrated polarization analyzing CMOS image sensor for autonomous agent navigation using polarized light. In: Proceedings of IEEE International conference on Intelligent Systems, pp. 224–229 (2010)
[34] Sarkar, M., Segundo, D.S., van Hoof, C., Theuwissen, A.: Integrated polarization analyzing CMOS image sensor for detecting incoming light ray direction. In: Proceedings of IEEE Sensors Application Symposium, pp. 194–199 (2010)
[35] Sarkar, M., Segundo, D.S., van Hoof, C., Theuwissen, A.: Biologically inspired autonomous agent navigation using stokes parameters and an integrated polarization analyzing CMOS image sensor. In: Proceedings of Eurosensors XXIV Conference, vol. 5, pp. 673–676 (2010)
[36] Gruev, V., van der Spiegel, J., Engheta, N.: Integrated polarization image sensor for cell detection. In: International Image Sensor Workshop (2009)
[37] Gruev, V., Perkins, R.: A 1 mpixel ccd image sensor with aluminum nanowire polarization filter. In: Proceedings of IEEE International Symposium on Circuits and Systems, pp. 629–632 (2010)
[38] Sarkar, M., Segundo, D.S., van Hoof, C., Theuwissen, A.J.P.: Integrated polarization analyzing CMOS for navigation and incoming light ray direction. In: IEEE Transactions of Instrumentation and Measurement (accepted for publication)
[39] Liu, W., Liu, S.: CMOS tunable 1/x circuit and its applications. Transactions on Fundamentals of Electronics, Communications and Computer Sciences E-86A, 1896–1899 (2003)
[40] Liu, W., Liu, S., Wei, S.K.: CMOS current-mode divider and its application. IEEE Transactions on Circuits and Systems-II 52(3), 145–148 (2005)